AGU100 ADVANCING EARTH AND SPACE SCIENCE

Geophysical Research Letters

RESEARCH LETTER
10.1029/2018GL078767

Key Points:
- Thickness of a seismogenic slip zone varies by an order of magnitude over tens of meters strike distance
- Thickness variations contain significant spatial structure with a correlation length scale of ~1 m and characteristic spacing of 2–4 m
- Characteristic spacing defines the dimension of contact asperities that weaken most efficiently by thermally activated mechanisms

Supporting Information:
- Supporting Information S1
- Data Set S1
- Data Set S2
- Data Set S3

Correspondence to:
J. D. Kirkpatrick,
james.kirkpatrick@mcgill.ca

Citation:
Kirkpatrick, J. D., Shervais, K. A. H., & Ronayne, M. J. (2018). Spatial variation in the slip zone thickness of a seismogenic fault. *Geophysical Research Letters*, *45*, 7542–7550. https://doi.org/10.1029/2018GL078767

Received 15 MAY 2018
Accepted 19 JUL 2018
Accepted article online 25 JUL 2018
Published online 14 AUG 2018

Spatial Variation in the Slip Zone Thickness of a Seismogenic Fault

J. D. Kirkpatrick[1], K. A. H. Shervais[2], and M. J. Ronayne[2]

[1]Department of Earth and Planetary Sciences, McGill University, Montréal, QC, Canada, [2]Department of Geoscience, Colorado State University, Fort Collins, CO, USA

Abstract Fault slip is predominantly localized onto narrow slip zones embedded within broader zones of fault rock and subsidiary damage. As earthquakes re-rupture the same slip zone multiple times, the composition and geometry of the slip zone significantly affect dynamic processes. Here we use three large cross-sectional exposures of an exhumed fault to show that the thickness of a slip zone that accommodated seismic slip varies by an order of magnitude over tens of meters along strike. Geostatistical analyses show that the thickness variations are characterized by a correlation length scale of ~1 m and a characteristic spacing of 2–4 m. We suggest that the spacing between regions of correlated thickness represents the dimension of contact asperities on the fault. Similar magnitude variations in slip zone thickness should be generic to faults in the brittle crust, implying that slip-weakening mechanisms such as thermal pressurization are spatially variable during seismic slip.

Plain Language Summary During an earthquake, rocks on either side of a fault slip past one another. At the interface between the moving rocks, the fault contains a layer of broken and ground up rock pieces. This layer is heated during the earthquake slip due to the friction between the rocks. If heated sufficiently, the layer can undergo physical or chemical changes that cause it to lubricate the fault, allowing the earthquake rupture to grow large. The rate of heating of the layer depends on properties such as heat capacity, and on the thickness of the layer—thinner layers heat faster than thicker layers. If the layer has variable thickness, then the heating and consequently lubrication effect will also be variable. In this study, we measured the layer thickness in an ancient fault now exposed at the Earth's surface, which experienced earthquakes in the past. Our high-resolution data show that the layer thickness is highly variable, but that the spatial pattern of the variability can be predicted statistically. These results allow us to predict how effectively faults are lubricated faults in regions experiencing earthquakes today, and improve our understanding of the physical processes that cause earthquakes deep in the Earth's crust.

1. Introduction

Slip zones are common components of exhumed faults. In the field they are defined by layers of the most comminuted fault rock (e.g., Sagy & Brodsky, 2009), are associated with polished slickenside surfaces exhibiting kinematic indicators (e.g., Smith et al., 2011), and demonstrate crosscutting relations with surrounding rocks (e.g., Wibberley & Shimamoto, 2005). Fault zones may contain one or multiple slip zones (Boullier et al., 2009; Caine & Forster, 1999). In both cases, slip zones can be shown to have accommodated a large proportion of the total displacement across a fault (Chester & Chester, 1998; Shipton & Cowie, 2001). Some slip zones contain clear evidence for deformation at seismic slip rates (Rowe & Griffith, 2015), but many lack diagnostic criteria for slip rate. As the locus of deformation within a fault, they are often associated with thicker accumulations of fault rock, often referred to as fault cores (Caine et al., 1996). Where the total offset across an individual slip zone is much greater than earthquake slip (i.e., $>10^1$ m), earthquakes are inferred to have ruptured individual slip zones repeatedly (e.g., Chester et al., 2005), with the total offset being an accumulation of many slip increments. Slip zone geometry, composition, and physical properties are therefore integral to fault strength, stability, and dynamic processes during earthquakes.

Dynamic weakening during earthquake slip is caused by processes that operate within slip zones. Weakening processes such as thermal pressurization, melting, and decarbonation (see reviews by Di Toro et al., 2011 and Rowe & Griffith, 2015) are thermally driven and are activated by frictional heating during slip. Hydraulic diffusivity of the slip zone and surrounding rocks is an important control on slip zone processes, but in general, narrow slip zones tend to promote weakening because the volume of the slip zone is relatively small

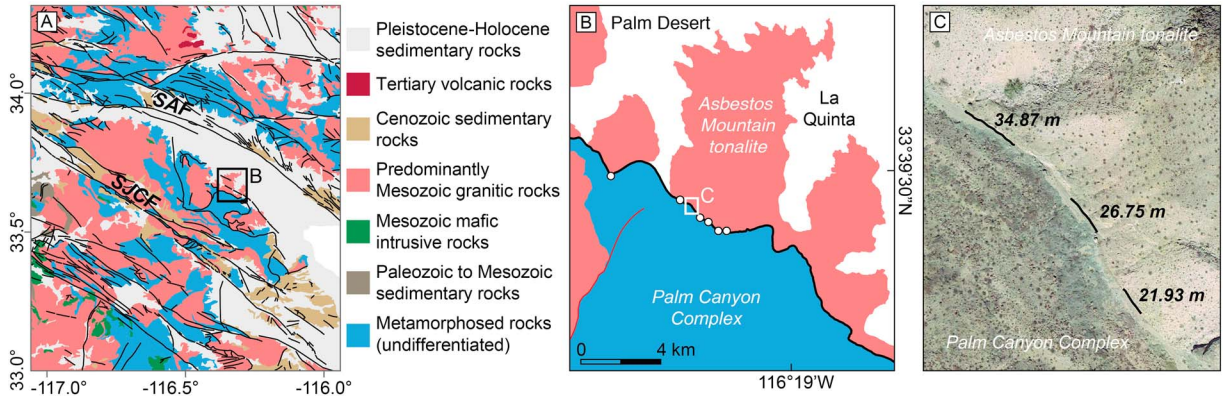

Figure 1. (a) Simplified geologic map of part of southern California (from Jennings et al., 2010) showing the location of the study area. Black lines are faults, SAF is San Andreas Fault, SJCF is the San Jacinto Fault, and box corresponds to location of (b). (b) Map showing the La Quinta fault in the study area. White circles represent exposures where layer *m* was identified. Location of (c) shown with white box. (c) Google Earth image showing locations of the three main exposures in which layer *m* was mapped in detail (black lines). Numbers adjacent to lines are the exposure lengths.

(e.g., Cardwell et al., 1978; Rice, 2006). Other potential weakening mechanisms, such as elastohydrodynamic lubrication (Brodsky & Kanamori, 2001) and gouge fluidization (Melosh, 1996; Otsuki et al., 2003), are less sensitive to temperature, but are dependent on variable slip zone thickness. Shear across nonuniform slip zones may also promote processes such as normal interface vibrations (Brune et al., 1993) and auto-acoustic compaction (van der Elst et al., 2012).

Slip surfaces, the three-dimensional surfaces that bound slip zones, have a characteristic geometry in which the roughness of the surface increases as a power law function of the length scale of observation (Brown & Scholz, 1985; Power et al., 1987; Sagy et al., 2007). This fractal behavior follows $H(L) = KL^{\zeta}$, where H is the RMS roughness evaluated over a portion of the fault with length scale, L; K is a constant; and ζ is the Hurst exponent, which for faults is observed to be <1 (Brodsky et al., 2016). Although some slip zones exhibit gradational contacts with surrounding fault rocks, the roughness of slip surfaces means that the thickness of a slip zone should be spatially variable unless there are slip surfaces on each side that are the same and exactly matched (Brown & Bruhn, 1996). Additionally, Scholz (1988) showed from consideration of closure of two elastic bodies bounded by fractal surfaces that flattening under load results in negligible aperture gaps for long-wavelength roughness and nonzero gaps at short wavelengths. If the gaps are filled with other material, such as gouge, then regions without gaps define contact asperities, areas of high resolved normal stress on a fault under in situ conditions. However, quantitative measures of the spatial relation between natural slip zones and slip surfaces are lacking, so relating fault structure to complexity in fault stress and earthquake slip distributions arising from "asperities" (Lay et al., 1982), remains challenging.

Slip zones are observed to range in thickness from microns to meters in ancient faults (Miller, 1996; Rowe et al., 2013; Shipton et al., 2006; Sibson, 2003), but few data are available to describe the spatial variation in thickness within a single fault. Here we take advantage of cross-sectional exposures through a seismogenic fault that contains a throughgoing slip zone that we interpret to have hosted earthquake slip. We mapped the zone at high resolution over tens of meters along strike and here use the data to characterize how the thickness varies spatially. The results reveal that the slip zone thickness is spatially correlated and constrain the dimension of asperities that control earthquake source dynamics.

2. Structural Setting

We mapped in detail the internal structure of the La Quinta Fault, located south of Palm desert, Southern California (Figure 1) (Shervais & Kirkpatrick, 2016). The La Quinta Fault has a mapped trace length of 9.4 km, an average dip of ~20°, and predominantly dip-slip motion indicated by slickenlines on exposed slip surfaces (Shervais & Kirkpatrick, 2016). It juxtaposes crystalline rocks of the amphibolite-grade Palm Canyon complex in the footwall and the Asbestos Mountain tonalite in the hanging wall (Sharp, 1979). The fault is exposed in a series of low cliffs that trend approximately parallel to strike. Thermochronologic data

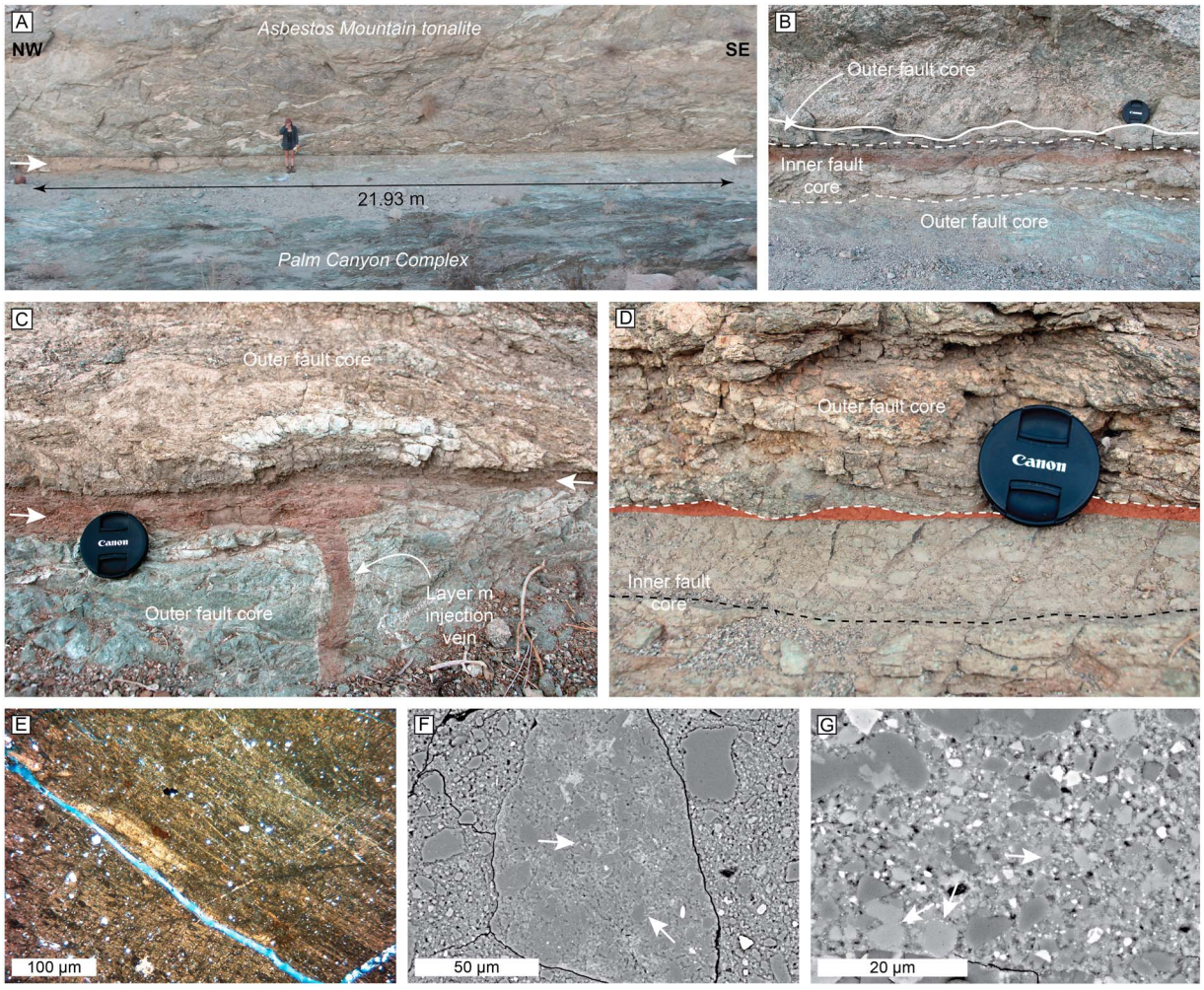

Figure 2. (a) Photograph of one of the exposures from which the internal structure of the La Quinta Fault was mapped. Fault core is between white arrows. (b) Representative photograph (not orthorectified) of the composite fault core. The inner fault core (between dashed lines) contains layers of ultracataclasite that crosscut fault rocks and other structures in the outer fault core. Layer *m* is too thin to see in this image. Solid white line marks the upper contact between the outer fault core and damage zone. All of the rock below the inner fault core is outer fault core cataclasite. (c) Detail of layer *m* (between white arrows) where it is relatively thick showing an injection vein branching down from the layer into the footwall (camera lens for scale ~60-mm diameter). In this part of the fault, layer *m* is the only layer present within the inner fault core. (d) Detail of layer *m* (highlighted in red) where it is relatively narrow. The upper edge of layer *m* is dashed in this image because it forms the upper edge of the inner fault core. Dashed black line indicates contact between other layers within inner fault core. (e) Photomicrograph (cross-polarized light) showing bands of grains with long axes aligned top left to bottom right and common extinction angle. (f) Scanning electron microscope back scattered electron (SEM-BSE) image showing clast (middle) of a relict pseudotachylyte in the ultracataclasite of layer *m*. Microcrystallites within the clast groundmass indicate the material inside the clast quenched from a molten state brought about by frictional heating during seismic slip (examples shown with white arrows). (g) SEM-BSE image of a different portion of the layer *m* groundmass where small clasts are mantled by metal oxide grains (white arrows).

indicate the fault was active as a reverse fault during the Laramide orogeny (Wenk et al., 2000), though numerous normal faults in the fault hanging wall that crosscut Laramide-aged pseudotachylytes indicate that the La Quinta Fault was reactivated as a low-angle normal fault post Laramide, possibly as part of the West Salton Detachment System (Axen & Fletcher, 1998; Shervais & Kirkpatrick, 2016). Total offset, as well as the offsets during different phases of deformation, is unknown due to a lack of piercing points.

The internal structure of the La Quinta Fault consists of a composite fault core flanked by a damage zone around 70 m wide defined by the presence of subsidiary faults and shear fractures (Figure 2). The fault core contains two components characterized by distinct fault rock assemblages: an outer fault core in which cataclasites and pseudotachylytes are derived from weakly altered hanging wall and footwall rocks and an inner fault core in which the degree of comminution is much greater and ultracataclasites contain chlorite, epidote, and smectite-group clays in larger abundances than the host rocks (Shervais & Kirkpatrick, 2016). The two

components are arranged so that the inner fault core is located centrally, with outer fault core rocks present on both sides.

The inner fault core contains 13 distinct layers of ultracataclasite. Where adjacent to the outer fault core, these layers crosscut the outer fault core, indicating that the inner fault core is younger. Each layer is distinguishable from the characteristics of the fault rocks within the layer, that is, the frequency, composition, and average size of clasts, as well as matrix color and grain size. Individual layer thickness varies from 0.1 to more than 40 cm. Evidence for truncation and wear of clasts within one layer by adjacent layers is common in the exposures we studied, and where exposed, the layer edges exhibit slickenlines. These observations suggest that each layer acted a slip zone at some stage during the deformation history of the fault and that the layers were bounded by slip surfaces. Relative ages of the layers were established by Shervais and Kirkpatrick (2016), but the lack of piercing points means that the proportion of the total fault offset accommodated across each is unknown. Due to the truncation and crosscutting, the layers are discontinuous along strike, except one (see below), and the number of layers present at a point within the inner fault core is variable.

One continuous layer within the inner fault core was identified in all exposures we studied, unlike any of the other layers. This layer, described as layer *m* by Shervais and Kirkpatrick (2016), was identified as the last slip zone active within the fault on the basis that it crosscuts and truncates all adjacent layers within the inner fault core, is the finest-grained layer within the fault, and is continuous over tens of meters. We observed this layer in multiple exposures spread over a 5-km distance. Layer *m* is texturally uniform and contains dark brown, extremely fine-grained ultracataclasite in which angular to rounded clasts range from <1 to ~100 μm (Figure 2). The ultracataclasite matrix is compositionally homogeneous, though in places phyllosilicate grains are observed to have parallel long axes (Figure 2d). Clasts are mostly fragments of wall rock minerals, though clasts of previously formed cataclasite and ultracataclasite are present, and some clasts of pseudotachylytes were observed with textures similar to those documented by Meneghini et al. (2010) (Figure 2e). In some regions where the layer matrix is completely granular, clasts <1 μm are indistinct and visible clasts are mantled by extremely fine (~100 nm) oxide grains (Figure 2f), which may be indicative of the local development of a low melt fraction, similar to that described by Otsuki et al. (2003). Injection veins filled with the same ultracataclasite as layer *m* branch from layer *m* at high angles to the overall fault orientation (Figure 2c). The injection veins are typically tens of centimeters long and are comparable thickness to layer *m* where they branch from it. Injection veins filled with ultracataclasite dissimilar to layer *m* are also present in the hanging wall, which we interpret to have formed during shear localized onto one of the other ultracataclasite layers in the inner fault core.

3. Slip Zone Thickness

The thickness of layer *m* varies from 0.1 to 8 cm (Figure 3). Thickness here is defined as the vertical separation between the upper and lower edges of the layer, as viewed in images orthorectified in the slip direction (where the layer edges are the intersection of the 3-D surfaces that bound the layer with the 2-D plane of the exposure). Maps of the layer geometry were constructed on high-resolution images (1.2 mm/pixel) generated from 3-D models created with structure-from-motion photogrammetry, which were scaled to the true dimension of the exposure using real-time kinematic (RTK) differential GPS ground control points (accurate to 1 mm horizontally and 2 mm vertically) (Shervais & Kirkpatrick, 2016). Three exceptional exposures of the La Quinta fault allowed layer *m* to be mapped continuously over along-strike distances of 34.87, 26.75, and 21.93 m, respectively. The edges of the layer follow a power law relation between roughness and length scale with a Hurst exponent ~0.8, consistent with fault slip surfaces measured in 3-D (Shervais & Kirkpatrick, 2016).

Spatial continuity is clear in the along-strike variations in layer *m* thickness. As shown in Figure 3, the thickest portions of the layer (~centimeters thick) are separated by portions several meters long in which the layer is relatively narrow (millimeters). We characterized this spatial variation in layer thickness by calculating the variogram, γ (*h*):

$$\gamma(\mathrm{h}) = \frac{1}{2\mathrm{N}(\mathrm{h})} \sum_{\mathrm{i}=1}^{\mathrm{N}} [\mathrm{t}(\mathrm{x}+\mathrm{h}) - \mathrm{t}(\mathrm{x})]^2$$

where *t* (*x*) represents the value of layer thickness (m) at a particular location *x*; *t* (*x* + *h*) is the value of the thickness at location *x* + *h*, where *h* is the separation distance, or lag (m); and *N* (*h*) is the number of data pairs

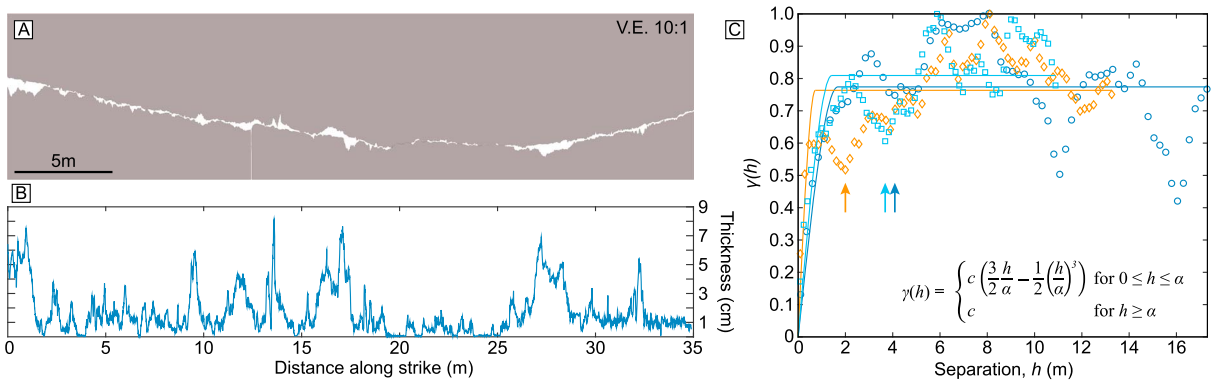

Figure 3. (a) Map of layer *m* in the largest studied exposure (represented as the white space between gray wall rocks). Note the vertical exaggeration of 10:1. (b) Plot of thickness (vertical separation in between the gray wall rocks in (a)) as a function of distance along the fault showing substantial thickness fluctuations. (c) Variograms calculated from the three layer *m* thickness data sets (values for each variogram are normalized to the maximum γ to facilitate comparison). Open symbols represent the experimental variogram, calculated directly from the thickness values in each data set. Solid lines represent a fitted variogram model, with model equation shown (*h* is the separation distance, α is the correlation distance, and *c* is the sill; α for each model fit reported in the main text). The correlation distance corresponds to the minimum *h* at which constant γ is reached. Location of first minimum in each variogram is shown by arrows.

(i.e., pairs of measured thickness values separated by *h*). For each data set (the three mapped exposures), we calculated the experimental variogram using lags in 70 linearly spaced bins from 0 to half the total exposure length, as γ (*h*) values at greater *h* would be informed by fewer pairs of data, making the calculated values less robust (Caers & Zhang, 2004).

In a stationary field, the value of γ (*h*) eventually reaches a constant value that is approximately equal to the variance of *t* (*x*) (Kitanidis, 1997). This constant value, or plateau on the variogram, is known as the sill. The distance at which the sill is reached is the correlation distance, α, often referred to as the range parameter. The range represents a characteristic distance beyond which separated values are, on average, no longer correlated; that is, closely spaced points are likely to be similar, whereas points separated by more than the correlation distance (~1 m) are independent of one another. The γ (*h*) values less than the sill for $h < \alpha$ indicate spatial structure in a data set. Fractal data sets, such as fault surfaces, result in γ (*h*) that increases continuously for all values of *h*. However, synthetic and natural fault core and vein thicknesses contain a finite length scale for the spatial correlation as the thicknesses of these structures have a known maximum value and do not continuously scale (Brown & Bruhn, 1996; Lunn et al., 2008).

Analysis of layer *m* shows that the layer contains significant spatial structure (Figure 3). In one exposure, the layer *m* thickness values have a positively skewed distribution, so we performed a log10-transformation of *t* (*x*) for calculation of the γ (*h*) to minimize the effect of extreme values in the data (Kerry & Oliver, 2007) (transformed data shown with diamond symbols in Figure 3c). Any linear trend over the range of *x* was subtracted from each data set, and occasional subcentimeter-sized gaps where injection veins branch from the layer were removed with a linear interpolation. We treat the thickness measurements as realizations of a spatial random function satisfying the intrinsic hypothesis (Kitanidis, 1997) and fit the calculated γ (*h*) values for the three exposures with a variogram model to estimate the correlation distances (Figure 3). Spherical and exponential variogram models both provided a good fit to the data. We selected a spherical model type, following the approach used in previous studies of fault core and vein thicknesses (Brown & Bruhn, 1996; Lunn et al., 2008). The models have correlation distances (i.e., fitted α values) of 1.7, 0.74, and 1.4 m.

In addition to the spatial continuity described by the variogram model, the spatial separation of thick regions of layer *m* by thin regions (Figure 3c) causes the value of γ (*h*) to fluctuate periodically around the sill. A characteristic spacing is defined as the separation distance at the first local minimum in the variogram (Herzfeld, 2008) (also roughly equal to the wavelength of γ (*h*) periodicity about the sill). Characteristic spacing is approximately 4.0, 2.0, and 3.7 m for the three exposures, respectively.

4. Discussion and Conclusions

Field-scale and microscale characteristics of the fault rocks within layer *m* indicate that the La Quinta Fault was seismogenic in the latest stages of faulting when layer *m* was the active slip zone (Shervais &

Kirkpatrick, 2016). Injection veins that branch from layer *m* are filled with the same ultracataclasite as the layer itself, which indicates that the fault rock was fluidized during seismic slip (Rowe et al., 2012). Clasts of relict pseudotachylyte are present within the layer, as well as locally developed textures that might indicate very low fraction melting at grain boundaries. Frictional melting therefore occurred at least once during past slip increments, including the last if the low melt fraction interpretation is correct, which requires slip at seismic slip rates. The microstructures of the layer *m* ultracataclasite also include aligned phyllosilicate grains within a chemically homogeneous layer, in which there is no sorting of grain size. Evidence for melting is not pervasive, and other weakening mechanism (s) that may have been active during the paleo-slip events are unconstrained by our microstructural observations. Mobilized gouge and grain alignment in layer *m* are consistent with, though not diagnostic of, thermal pressurization, elastohydrodynamic lubrication, and flash weakening, for example. We were unable to find evidence of localization within layer *m* (or other layers) based on optical and scanning electron microscope observations, so we interpret shear to have been distributed across the entire thickness of the layer during slip.

The thickness of layer *m* varies by an order of magnitude over along-strike distances of tens of meters. As the correlation distances (α) for each exposure are quite similar, we suggest that they represent the same physical property of layer *m*. Differences in in the α values estimated in different exposures are likely due to random variations in the thicknesses (consistent with a stochastic process). Periodicity is present in each of the three variograms, and the characteristic spacing is also similar for the three exposures. The characteristic spacing is the spacing between regions of spatially correlated data with similar mean values (e.g., the distance between midpoints of two thin regions separated by an interval where the layer is thick).

Geostatistical analyses of the aperture between synthetic fractal surfaces laterally offset from an initial matched condition show that the apertures contain spatial structure defined by a range and sill in the variogram, where the range is approximately the shear offset (Brown & Bruhn, 1996). We do not know the original degree of mismatch across layer *m*, but it is possible that the correlation length scale observed for layer *m* results from a small strike-slip component of net offset across the layer indicated by slickenline rakes. However, the results of Brown and Bruhn (1996) did not include any elastic closure due to normal load across the fault, or effects of cataclastic deformation and wear during fault offset, which were significant for the La Quinta fault and may have modified the surfaces bounding layer *m* after formation (Shervais & Kirkpatrick, 2016), so relating the correlation length scale to lateral offset is likely an oversimplification.

The data presented in Figure 3 define the variation in slip zone thickness viewed in a plane perpendicular to slip. Surveys of the 3-D geometry of fault slip surfaces show that they are smoother in the slip-parallel direction (smaller values for *K*) compared to slip-perpendicular, with Hurst exponents of ~0.6 and ~0.8 in the two directions, respectively (Brodsky et al., 2016). Hurst exponents have been shown to be relatively constant across tectonic settings and rock types, and as the surfaces that bound layer *m* are consistent with these values in the slip-perpendicular direction (Shervais & Kirkpatrick, 2016), we expect the slip-parallel direction to also share these characteristics. This implies that layer *m* has rough edges, and a variable thickness, in the slip direction. The slip-parallel minimum and maximum values of the layer thickness are similar to variations in the strike direction, but as the layer edges would be smoother with smaller *H* in the slip-parallel direction, the thin regions of the layer are likely larger (e.g., Campaná et al., 2008). Without exposure in the slip direction, we cannot measure the correlation length scales and characteristic separation. However, as the power law scaling of fault surface roughness with length scale is a fundamental characteristic of fault slip surfaces (Brodsky et al., 2016), layer thickness variations should be a common feature of all faults.

The characteristic spacing of the slip zone thickness is an important length scale in a fault, and may be considered as one definition of an "asperity." As fault rock similar to that within layer *m* has low stiffness compared to the surrounding material (Chester & Logan, 1986), opposing sides of a fault are effectively in contact in areas of very thin or negligible slip zone thickness (Nielsen et al., 2010). In this case, the spacing of regions with narrow apertures (i.e., layer thickness) between the two sides of a fault is a characteristic length for the fault. The characteristic spacing defined by the variogram periodicity measures this length scale. The fractal shape of slip surfaces means that smaller asperities may be expected if higher-resolution data were collected. However, additional high-resolution data would add more detail to the form of the

variogram at short separation distances, but would not change the large-separation distance behavior. Scholz (1988) showed that the closure of long-wavelength apertures in a fault zone under load causes all wavelengths above a characteristic length to be closed, while shorter-wavelength apertures may not be. These characteristics may be apparent in Figure 3a, where an overall sinusoidal shape to both the upper and lower edges of the slip zone are very well matched.

Slip zone thickness is a key parameter for a variety of slip weakening mechanisms, in particular thermally activated mechanisms (Rice, 2006). To illustrate the implications of our observations for rupture dynamics, we explore the effects of spatially variable slip zone thickness on thermal pressurization. Viesca and Garagash (2015) demonstrate that in the early stages of slip immediately following rupture propagation, the evolution of effective normal stress due to thermal pressurization is characterized by two slip distances, δ_c and L^*. Parameter δ_c is the slip over which the fault behaves as an intact undrained, adiabatic system and is directly proportional to the slip zone thickness. L^* is a measure of the slip sufficient for diffusion of fluid and heat to become significant and the fault to act as a damaged system characterized by slip on a plane behavior. It is most sensitive to hydraulic and thermal diffusivities, but not layer thickness (Viesca & Garagash, 2015). The efficiency of thermal pressurization, a measure of how rapidly strength is reduced during slip immediately behind a propagating rupture tip, is given by the ratio L^*/δ_c.

Assuming that shear was distributed across the entire thickness of layer *m* during seismic slip on the La Quinta Fault, the observed spatial variation in thickness of the layer (1 to 80 mm) indicates that L^*/δ_c would vary by an order of magnitude over on-fault distances of 10^1 m. Areas of the fault where layer *m* was thin (dimension corresponding to the characteristic spacing) were contacts that supported high normal loads, but within which thermal pressurization would be very efficient, reducing effective normal stresses over relatively short slip distances. Strength reduction would be less efficient in areas where the layer was thick. Slip greater than the characteristic spacing in the layer thickness would cause long-wavelength apertures to open as the degree of mismatch increased. This length scale may therefore represent the slip required to transition from an intact to damaged fault zone (Viesca & Garagash, 2015). A similar dimension (of the order of 1 m) has been defined from the lengths of laterally discontinuous pseudotachylytes in exhumed seismogenic strike-slip faults (Kirkpatrick & Shipton, 2009). In the earthquake fracture energy-slip compilation presented by Viesca and Garagash (2015), the transition away from an intact fault occurs at around 10^0 m.

In conclusion, we have shown that slip zone thickness is spatially variable within a seismogenic fault. Our results demonstrate that the correlation length scale that describes the spatial variation in slip zone thickness has values of ~1 m, with a characteristic spacing between regions in which the layer has similar mean values of ~2–4 m. We suggest that this spacing represents the dimension of a contact asperity on the fault. Due to the variations in slip zone thickness, slip-weakening mechanisms such as thermal pressurization must have been spatially variable during paleo-seismic slip on the La Quinta Fault, with higher efficiency in regions of narrow slip zone. Our observations therefore indicate that static fault strength is determined by meter-scale contact asperities, which weaken most rapidly during seismic slip.

Acknowledgments
We thank Allan Muth and the UC Riverside Boyd Deep Canyon Nature Reserve for field access and sampling permission. Thanks also to Gavin Medley, Jonathan Caine, and Robert Viesca for their helpful conversations during the study and to Fred Chester and Chris Marone for the thorough and constructive reviews that substantially improved the manuscript. Thickness measurements are included in the supporting information. This work was supported in part by the Southern California Earthquake Center (award 14074). SCEC is funded by NSF cooperative agreement EAR-1033462 and USGS cooperative agreement G12AC20038.

References

Axen, G. J., & Fletcher, J. M. (1998). Late Miocene Pleistocene extensional faulting, northern gulf of California, Mexico and Salton trough, California. *International Geology Review*, *40*(3), 217–244. https://doi.org/10.1080/00206819809465207

Boullier, A. M., Yeh, E. C., Boutareaud, S., Song, S. R., & Tsai, C. H. (2009). Microscale anatomy of the 1999 Chi-Chi earthquake fault zone. *Geochemistry, Geophysics, Geosystems*, *10*(3), Q03016. https://doi.org/10.1029/2008GC002252

Brodsky, E. E., & Kanamori, H. (2001). Elastohydrodynamic lubrication of faults. *Journal of Geophysical Research*, *106*(B8), 16,357–16,374. https://doi.org/10.1029/2001JB000430

Brodsky, E. E., Kirkpatrick, J. D., & Candela, T. (2016). Constraints from fault roughness on the scale-dependent strength of rocks. *Geology*, *44*(1), 19–22. https://doi.org/10.1130/g37206.1

Brown, S. R., & Bruhn, R. L. (1996). Formation of voids and veins during faulting. *Journal of Structural Geology*, *18*(5), 657–671. https://doi.org/10.1016/s0191-8141(96)80031-9

Brown, S. R., & Scholz, C. H. (1985). Broad bandwidth study of the topography of natural rock surfaces. *Journal of Geophysical Research*, *90*(B14), 12,575–12,582. https://doi.org/10.1029/JB090iB14p12575

Brune, J. N., Brown, S., & Johnson, P. A. (1993). Rupture mechanism and interface separation in foam rubber models of earthquakes—A possible solution to the heat-flow paradox and the paradox of large overthrusts. *Tectonophysics*, *218*(1–3), 59–67. https://doi.org/10.1016/0040-1951(93)90259-M

Caers, J., & Zhang, T. (2004). Multiple-point geostatistics: A quantitative vehicle for integrating geologic analogs into multiple reservoir models. In *Integration of Outcrop and Modern Analogs in Reservoir Modeling* (pp. 383–394). American Association of Petroleum Geologists.

Caine, J. S., Evans, J. P., & Forster, C. B. (1996). Fault zone architecture and permeability structure. *Geology*, *24*(11), 1025–1028. https://doi.org/10.1130/0091-7613(1996)024<1025:FZAAPS>2.3.CO;2

Caine, J. S., & Forster, C. B. (1999). Fault zone architecture and fluid flow: Insights from field data and numerical modeling. *Geophysical Monograph-American Geophysical Union*, *113*, 101–128.

Campaná, C., Müser, M. H., & Robbins, M. O. (2008). Elastic contact between self-affine surfaces: Comparison of numerical stress and contact correlation functions with analytic predictions. *Journal of Physics: Condensed Matter*, *20*(35), 354013.

Cardwell, R. K., Chinn, D. S., Moore, G. F., & Turcotte, D. L. (1978). Frictional heating on a fault zone with finite thickness. *Geophysical Journal of the Royal Astronomical Society*, *52*(3), 525–530. https://doi.org/10.1111/j.1365-246X.1978.tb04247.x

Chester, F. M., & Chester, J. S. (1998). Ultracataclasite structure and friction processes of the punchbowl fault, San Andreas system, California. *Tectonophysics*, *295*(1–2), 199–221. https://doi.org/10.1016/S0040-1951(98)00121-8

Chester, F. M., & Logan, J. M. (1986). Implications for mechanical-properties of brittle faults from observations of the punchbowl fault zone, California. *Pure and Applied Geophysics*, *124*(1–2), 79–106.

Chester, J. S., Chester, F. M., & Kronenberg, A. K. (2005). Fracture surface energy of the punchbowl fault, San Andreas system. *Nature*, *437*(7055), 133–136. https://doi.org/10.1038/nature03942

Di Toro, G., Han, R., Hirose, T., De Paola, N., Nielsen, S., Mizoguchi, K., et al. (2011). Fault lubrication during earthquakes. *Nature*, *471*(7339), 494. https://doi.org/10.1038/nature09838

Herzfeld, U. C. (2008). Master of the obscure—Automated geostatistical classification in presence of complex geophysical processes. *Mathematical Geosciences*, *40*(5), 587–618. https://doi.org/10.1007/s11004-008-9174-4

Jennings, C. W., Gutierrez, C., Bryant, W., Saucedo, G., & Wills, C. (2010). Geologic map of California: California geological survey, Geologic Data Map No. 2, scale 1:750,000.

Kerry, R., & Oliver, M. A. (2007). Determining the effect of asymmetric data on the variogram. *II. Outliers, Computers & Geosciences*, *33*(10), 1233–1260. https://doi.org/10.1016/j.cageo.2007.05.009

Kirkpatrick, J. D., & Shipton, Z. K. (2009). Geologic evidence for multiple slip weakening mechanisms during seismic slip in crystalline rock. *Journal of Geophysical Research*, *114*, B12401. https://doi.org/10.1029/2008JB006037

Kitanidis, P. K. (1997). *Introduction to Geostatistics: Applications in Hydrogeology*. Cambridge University Press. https://doi.org/10.1017/CBO9780511626166

Lay, T., Kanamori, H., & Ruff, L. (1982). The asperity model and the nature of large subduction zone earthquakes. *Earthquake Prediction Research*, *1*(1), 3–71.

Lunn, R. J., Shipton, Z. K., & Bright, A. M. (2008). How can we improve estimates of bulk fault zone hydraulic properties? *Geological Society, London, Special Publications*, *299*(1), 231–237. https://doi.org/10.1144/SP299.14

Melosh, H. J. (1996). Dynamical weakening of faults by acoustic fluidization. *Nature*, *379*(6566), 601–606. https://doi.org/10.1038/379601a0

Meneghini, F., Di Toro, G., Rowe, C. D., Moore, J. C., Tsutsumi, A., & Yamaguchi, A. (2010). Record of mega-earthquakes in subduction thrusts: The black fault rocks of Pasagshak point (Kodiak Island, Alaska). *Geological Society of America Bulletin*, *122*(7–8), 1280–1297. https://doi.org/10.1130/b30049.1

Miller, M. G. (1996). Ductility in fault gouge from a normal fault system, Death Valley, California: A mechanism for fault-zone strengthening and relevance to paleoseismicity. *Geology*, *24*(7), 603–606. https://doi.org/10.1130/0091-7613(1996)024<0603:DIFGFA>2.3.CO;2

Nielsen, S., Di Toro, G., & Griffith, W. A. (2010). Friction and roughness of a melting rock surface. *Geophysical Journal International*, *182*(1), 299–310. https://doi.org/10.1111/j.1365-246X.2010.04607.x

Otsuki, K., Monzawa, N., & Nagase, T. (2003). Fluidization and melting of fault gouge during seismic slip: Identification in the Nojima fault zone and implications for focal earthquake mechanisms. *Journal of Geophysical Research*, *108*(B4), 2192. https://doi.org/10.1029/2001JB001711

Power, W. L., Tullis, T. E., Brown, S. R., Boitnott, G. N., & Scholz, C. H. (1987). Roughness of natural fault surfaces. *Geophysical Research Letters*, *14*(1), 29–32. https://doi.org/10.1029/GL014i001p00029

Rice, J. R. (2006). Heating and weakening of faults during earthquake slip. *Journal of Geophysical Research*, *111*, B05311. https://doi.org/10.1029/2005JB004006

Rowe, C. D., & Griffith, W. A. (2015). Do faults preserve a record of seismic slip: A second opinion. *Journal of Structural Geology*, *78*, 1–26. https://doi.org/10.1016/j.jsg.2015.06.006

Rowe, C. D., Kirkpatrick, J. D., & Brodsky, E. E. (2012). Fault rock injections record paleo-earthquakes. *Earth and Planetary Science Letters*, *335-336*, 154–166. https://doi.org/10.1016/j.epsl.2012.04.015

Rowe, C. D., Moore, J. C., Remitti, F., & Scientist, I. E. T. (2013). The thickness of subduction plate boundary faults from the seafloor into the seismogenic zone. *Geology*, *41*(9), 991–994. https://doi.org/10.1130/g34556.1

Sagy, A., & Brodsky, E. E. (2009). Geometric and rheological asperities in an exposed fault zone. *Journal of Geophysical Research*, *114*, B02301. https://doi.org/10.1029/2008JB005701

Sagy, A., Brodsky, E. E., & Axen, G. J. (2007). Evolution of fault-surface roughness with slip. *Geology*, *35*(3), 283–286. https://doi.org/10.1130/g23235a.1

Scholz, C. H. (1988). The critical slip distance for seismic faulting. *Nature*, *336*(6201), 761–763. https://doi.org/10.1038/336761a0

Sharp, R. V. (1979). Some characteristics of the eastern Peninsular Ranges mylonite zone. *Reproducción*, 258–267.

Shervais, K. A. H., & Kirkpatrick, J. D. (2016). Smoothing and re-roughening processes: The geometric evolution of a single fault zone. *Journal of Structural Geology*, *91*, 130–143. https://doi.org/10.1016/j.jsg.2016.09.004

Shipton, Z. K., & Cowie, P. A. (2001). Damage zone and slip-surface evolution over mu m to km scales in high-porosity Navajo sandstone, Utah. *Journal of Structural Geology*, *23*(12), 1825–1844. https://doi.org/10.1016/S0191-8141(01)00035-9

Shipton, Z. K., Soden, A. M., Kirkpatrick, J. D., Bright, A. M., & Lunn, R. J. (2006). How thick is a fault? Fault displacement-thickness scaling revisited. In R. E. Abercrombie, A. McGarr, G. di Toro, & H. Kanamori (Eds.), *Earthquakes: Radiated Energy and the Physics of Faulting* (pp. 193–198). American Geophysical Union.

Sibson, R. H. (2003). Thickness of the seismic slip zone. *Bulletin of the Seismological Society of America*, *93*(3), 1169–1178. https://doi.org/10.1785/0120020061

Smith, S. A. F., Billi, A., Di Toro, G., & Spiess, R. (2011). Principal slip zones in limestone: Microstructural characterization and implications for the seismic cycle (Tre Monti fault, central Apennines, Italy). *Pure and Applied Geophysics*, *168*(12), 2365–2393. https://doi.org/10.1007/s00024-011-0267-5

van der Elst, N. J., Brodsky, E. E., Le Bas, P. Y., & Johnson, P. A. (2012). Auto-acoustic compaction in steady shear flows: Experimental evidence for suppression of shear dilatancy by internal acoustic vibration. *Journal of Geophysical Research*, *117*, B09314. https://doi.org/10.1029/2011JB008897

Viesca, R. C., & Garagash, D. I. (2015). Ubiquitous weakening of faults due to thermal pressurization. *Nature Geoscience*, *8*(11), 875. https://doi.org/10.1038/ngeo2554

Wenk, H. R., Johnson, L. R., & Ratschbacher, L. (2000). Pseudotachylites in the eastern peninsular ranges of California. *Tectonophysics*, *321*(2), 253–277. https://doi.org/10.1016/S0040-1951(00)00064-0

Wibberley, C. A. J., & Shimamoto, T. (2005). Earthquake slip weakening and asperities explained by thermal pressurization. *Nature*, *436*(7051), 689–692. https://doi.org/10.1038/nature03901